Acta Biomaterialia xxx (2017) xxx–xxx

Contents lists available at ScienceDirect

Acta Biomaterialia

journal homepage: www.elsevier.com/locate/actabiomat

Full length article

The effects of surface processing on *in-vivo* corrosion of Nitinol stents in a porcine model

Stacey J.L. Sullivan [a], Daniel Madamba [b], Shiril Sivan [a], Katie Miyashiro [b], Maureen L. Dreher [a], Christine Trépanier [b], Srinidhi Nagaraja [a,*]

[a] *U.S. Food and Drug Administration, Center for Devices and Radiological Health, Office of Science and Engineering Laboratories, Division of Applied Mechanics, Silver Spring, MD 20993, USA*
[b] *Confluent Medical Technologies, Fremont, CA 94539, USA*

ARTICLE INFO

Article history:
Received 12 May 2017
Received in revised form 17 August 2017
Accepted 21 August 2017
Available online xxxx

Keywords:
Corrosion
Stents
Nitinol
In-vivo
In-vitro
Explant

ABSTRACT

A major limitation with current assessments of corrosion in metallic medical devices is the lack of correlation between *in-vitro* and *in-vivo* corrosion performance. Therefore, the objective of this study was to elucidate the relationship between pitting corrosion measured by breakdown potentials (E_b) in ASTM F2129 testing and corrosion resistance *in-vivo*. Four groups of Nitinol stents were manufactured using different processing methods to create unique surface properties. The stents were implanted into iliac arteries of minipigs for six months and explanted for corrosion analysis. Scanning electron microscopy and energy dispersive X-ray spectrometry analyses indicated that stents with a thick complex thermal oxide (420 nm) and high corrosion resistance *in-vitro* (E_b = 975 ± 94 mV) were free from detectable corrosion *in-vivo* and exhibited no changes in Ni/Ti ratio when compared to non-implanted controls. This result was also found in mechanically polished stents with a thin native oxide (4 nm; E_b = 767 ± 226 mV). In contrast, stents with a moderately thick thermal oxide (130 nm) and low corrosion resistance *in-vitro* (E_b = 111 ± 63 mV) possessed corrosion with associated surface microcracks *in-vivo*. In addition, Ni/Ti ratios in corroded regions were significantly lower compared to non-corroded adjacent areas on explanted stents. When stents were minimally processed (i.e. retained native tube oxide from the drawing process), a thick thermal oxide was present (399 nm) with low *in-vitro* corrosion resistance (E_b = 68 ± 29 mV) resulting in extensive *in-vivo* pitting. These findings demonstrate that functional corrosion testing combined with a detailed understanding of the surface characteristics of a Nitinol medical device can provide insight into *in-vivo* corrosion resistance.

Statement of Significance

Nitinol is a commonly used material in the medical device industry. However, correlations between surface processing of nitinol and *in-vivo* corrosion has yet to be established. Elucidating the link between *in-vivo* corrosion and pre-clinical characterization can aid in improved prediction of clinical safety and performance of nitinol devices. We addressed this knowledge gap by fabricating nitinol stents to possess distinct surface properties and evaluating their corrosion susceptibility both *in-vitro* and after six months of *in-vivo* exposure. Relationships between stent processing, surface characterization, corrosion bench testing, and outcomes from explanted devices are discussed. These findings highlight the importance of surface characterization in nitinol devices and provide *in-vitro* pitting corrosion levels that can induce *in-vivo* corrosion in nitinol stents.

Published by Elsevier Ltd on behalf of Acta Materialia Inc.

1. Introduction

The corrosion resistance of medical implant alloys has increased over the past few decades due to advancements in manufacturing technologies. Even with these improvements, corrosion of biomedical materials has been reported for both orthopaedic and cardio-

* Corresponding author at: U.S. Food and Drug Administration, Center for Devices and Radiological Health, 10903 New Hampshire Avenue, Building 62, Room 2210, Silver Spring, MD 20993-0002 USA.
E-mail address: srinidhi.nagaraja@fda.hhs.gov (S. Nagaraja).

http://dx.doi.org/10.1016/j.actbio.2017.08.029
1742-7061/Published by Elsevier Ltd on behalf of Acta Materialia Inc.

vascular devices. Several recent research studies found corrosion damage in titanium and cobalt-chromium alloys from explanted metal-on-metal hip replacement devices [1–5]. Corrosion has also been observed in other orthopaedic implants such as screws and wires made from stainless steel alloys [6–8]. Corrosion in cardiovascular devices has been documented to a lesser extent mainly due to difficulties in obtaining explants for these life supporting implants. Two studies reported severe pitting corrosion in first generation Nitinol endovascular grafts in as little as 5 months of implantation time [9,10]. Brott and colleagues recently found corrosion in explanted cardiovascular stents made of Nitinol, stainless steel, and cobalt based alloys [11–13]. However, these studies predominantly identified corrosion qualitatively through microscopy and did not have matched controls to definitively distinguish *in-vivo* corrosion from pre-existing features from the manufacturing process.

Significant corrosion from medical implant material may not only adversely affect the structure or function of the device, but also provoke a biological response. Corrosion in orthopaedic metallic hip replacement devices has resulted in pseudotumors and adverse local tissue reactions [14–18]. For cardiovascular devices, the biological consequences of corrosion byproducts are less clear as metal ions may be transported systemically by blood flow or remain locally within the vascular tissues. Corrosion byproducts in cardiovascular stents can elicit an inflammatory cell response that increases neointimal growth in the vessel that results in restenosis [19,20]. This is especially important for Nitinol implants because approximately half of the elemental composition is nickel which has been shown to cause allergic reactions, nephrotoxicity, and carcinogenicity at various doses [21–24]. It should be noted that while hypersensitivity-related adverse events (e.g. contact dermatitis) have been reported in cardiovascular implants [25–32], a direct causal link between corrosion and these adverse events has yet to be established. Research studies that can more directly identify the ramifications of corrosion in medical implant biomaterials, particularly those that contain nickel, would help address this critical knowledge gap.

To aid medical device manufacturers in non-clinical corrosion assessment of cardiovascular metallic stents, the US Food and Drug Administration recently published an update to the guidance document (Select Updates for Non-Clinical Engineering Tests and Recommended Labeling for Intravascular Stents and Associated Delivery Systems: Guidance for Industry and Food and Drug Administration Staff). The *in-vitro* testing paradigm outlined in the guidance document recommends cyclic potentiodynamic polarization testing per ASTM F2129 (Standard Test Method for Conducting Cyclic Potentiodynamic Polarization Measurements to Determine the Corrosion Susceptibility of Small Implant Devices). This bench test method evaluates the voltage required to initiate pitting on the device surface (i.e. breakdown potential). If the pre-specified acceptance criterion is not met, additional *in-vitro* testing such as nickel leach testing or surface characterization is recommended. In 2007, acceptance criteria for ASTM F2129 testing were proposed by Rosenbloom and Corbett, suggesting that implants with a breakdown potential exceeding 600 mV have acceptable performance, potentials below 300 mV are unacceptable, and potentials between 300 and 600 mV may be acceptable if certain conditions are met [33]. These criteria were based primarily on previous studies that found rest potentials varied for stainless steel alloys (−380 to 290 mV) [34,35], Nitinol (−400 to −100 mV) [35,36] and cobalt-chromium alloys (−100 to 150 mV) [37] in various anatomic locations. Although rest and breakdown potentials from ASTM F2129 are used to assess pitting corrosion resistance during regulatory review of medical device applications, there is considerable debate within the medical device community regarding the relevance of the proposed acceptance criteria [38,39]. In fact, members of the cardiovascular implant community cited the lack of *in-vivo* performance correlation with current bench corrosion testing (e.g. ASTM F2129 testing) as a major limitation [40]. This is especially important for Nitinol implants because the corrosion resistance of Nitinol is highly dependent on the manufacturing processes. Therefore, the objective of this study was to characterize the relationship between *in-vitro* performance and *in-vivo* corrosion for Nitinol stents manufactured to span the full range of ASTM F2129 breakdown potentials. The selected stent groups included contrasting *in-vitro* performance to elucidate potential disparities *in-vivo*.

2. Methods

2.1. Stent manufacturing and characterization

Nitinol stents (8 mm × 30 mm length) were manufactured using a generic design by Confluent Medical Technologies. To investigate the effects of surface finish on *in-vitro* and *in-vivo* corrosion, four unique surface conditions were created using different processing methods: Salt Pot (SP), Mechanical Polish (MP), Air Furnace (AF), and Oxidized Tube (OT). Table 1 provides a summary of these methods that have been previously described in detail [41]. Depth profiles of surface constituents (n = 1 stent/group) were captured through Auger Electron Spectroscopy (PHI 680, Physical Electronics, East Chanhassen, MN) by alternating an acquisition cycle with a sputter cycle. The oxide layer thickness was determined by using the full width at half maximum method.

2.2. Potentiodynamic polarization testing

In-vitro pitting corrosion resistance of stents (n = 14 for SP, MP, and AF stent groups and n = 8 for OT stents) was characterized per ASTM F2129. Gamry (Interface 1000, Warminister, PA) or Princeton Applied Research (Model 263A, Oak Ridge, TN) potentiostats were used for all corrosion susceptibility assessments. Saturated Calomel Electrode (SCE) was used as a reference electrode and graphitic carbon was used as an counter electrode. Stents were tested in phosphate buffered saline (PBS, deaerated with nitrogen gas at 150 cm^3/min for 30 min) at a temperature of 37 ± 2 °C. The rest potential (E_r) was recorded after the stents had been submerged in PBS for one hour and then the potentiodynamic scan was initiated in the positive direction at a scan rate of 1 mV/s. The potential at which the current rapidly increases by 100× was established as the breakdown potential (E_b). If the stent did not experience breakdown during testing, the E_b was considered to be the vertex potential (1000 mV). The scan was reversed at 1000 mV or if the current densities exceeded 25 mA. The over potential was calculated as the difference between the breakdown potential and the rest potential (E_b–E_r).

2.3. Stent implantations

Stent implantations and animal husbandry were conducted at MedStar Health Research Institute (MHRI) under an approved Institutional Animal Care and Use Committee (IACUC) protocol (#2012-022) in accordance with the principles of the Animal Welfare Act and the NIH guidelines established for the Care and Use of Laboratory Animals. Female Yucatan miniature swine (minipigs, Sinclair BioResources, Auxvasse, MO) approximately 1 year of age and 50 kg were chosen for use in this study due to their established suitability as a long term animal model for cardiovascular device implantation [42–45]. All stents used for implantation were sterilized using Ethylene Oxide (EtO) as it is commonly used to sterilize stents and has been shown not to impact the corrosion resistance

Table 1
Stent manufacturing processes.

Group	SP	MP	AF	OT
Tubing	Ground (OD*)	Ground (OD*)	Ground (OD*)	As -received
	Honed (ID*)	Honed (ID*)	Honed (ID*)	
	Laser Cut	Laser Cut	Laser Cut	Laser Cut
Heat Affected Zone	Honed (ID*)	Honed (ID*)	Honed (ID*)	No processing
	Debur & Desludge	Debur & Desludge	Debur & Desludge	
	Chemically Polish	Chemically Polish	Chemically Polish	
Stress Relief	505°C Salt Pot	505°C Salt Pot	540°C Air furnace	505°C Salt Pot
Expansion	505°C Salt Pot	505°C Salt Pot	505°C Air furnace	505°C Salt Pot
AF Tuning	505°C Salt Pot	505°C Salt Pot	550°C Air furnace	505°C Salt Pot
Finishing	Ultrasonic clean	Ultrasonic clean	Ultrasonic clean	
		Chemical Etch		
		Chemical Polish		
		Burnish (OD*, 400 grit)		
		Ultrasonic clean		
Visual Appearance				
Oxide Layer Thickness (nm)	420	4	130	399

* process only applies to surface indicated ("OD" outer diameter or "ID" inner diameter).

of nitinol [46]. Prior to implantation, contrast enhanced angiography (Integris, Phillips, Andover, MA) was performed in orthogonal views (left anterior oblique and/or right anterior oblique) to select the target location within the iliac artery based on adequate diameter and length. Stents were implanted under fluoroscopic guidance into the iliac arteries in 12 minipigs (n = 3 per stent group: SP, MP, AF, and OT). A second angiogram was taken after stent deployment to confirm appropriate placement (Fig. S1). The stent oversizing (deployed diameter/native diameter) for this cohort was 1.12 ± 0.09, which is similar to clinical oversizing of Nitinol stents and has been previously shown not to elicit adverse biological responses in minipigs [47]. During the implantation period, animals were fed a commercial pelleted chow diet (Teklad Mini Swine Diet 8753C, Envigo, Indianapolis, IN) and tap water ad libitum. All animals were given 81 mg aspirin and 75 mg clopidogrel bisulfate daily for the duration of the study.

After a 6-month implantation period, minipigs were euthanized with potassium chloride administered by intravenous infusion. A veterinarian performed a comprehensive necropsy and found that stented vessels and adjacent tissue did not have visible trauma (e.g. perforation, bruising, tearing, discoloration, or hemorrhage) for any animal. In addition, examination of orifices, thoracic and abdominal cavities revealed that minipigs were healthy (no inflammation, infection, infarction or other systemic abnormalities) with the exception of one MP and SP animal, which were noted to have an enlarged inguinal lymph node with the contralateral lymph node normal in appearance. The treated vessels were removed intact and a suture was tied to the proximal end of the stent to maintain orientation. The vessels were gravity flushed with heparinized Lactated Ringer's Solution (2 mL heparin in 1 L of Lactated Ringer's Solution) to remove blood residues, and then perfusion fixed with 10% neutral buffered formalin (NBF). All tools and containers used during the handling of the explants and tissue removal process were non-metallic and acid washed to avoid metal ion contamination. Vascular tissue surrounding explanted stents was removed by digestion under gentle agitation at 60 ± 2 °C with a papain based tissue digestion solution. Papain was chosen to digest tissue from the explanted stented arteries based on previous results demonstrating papain does not significantly alter Nitinol stent surfaces [48]. When no visible tissue remained, the stent was transferred to a new container and rinsed for one hour in ultra-pure DI water. Stents were then air dried and stored in individually labeled tubes for subsequent corrosion analysis.

2.4. Explanted stent analysis

The entire length of each explanted stent was inspected using scanning electron microscopy (SEM) (JSM-6390LV, JOEL USA, Inc., Peabody, MA) to characterize and compare stent morphology and features of explanted stents to as-received non-implanted stents (baseline). Baseline stents were from the same manufacturing lot as implanted stents and also EtO sterilized. The abluminal (outer surface of stent), laser cut side wall, and luminal (inner surface of the stent) surface of stents were inspected for corrosion and surface damage. As a complimentary means to identify areas of localized corrosion, energy dispersive X-ray spectrometry (EDS) (NORAN System SIX v1.8, Thermo Electron, Waltham, MA) was used to identify constituents on the abluminal surface in visually corroded regions and non-corroded regions (parameter settings: 600×, 20 kV, 10–12 mm working distance, 15–25 s dead time). The weight% ratio of nickel to titanium (Ni/Ti) was calculated from EDS spectra in explanted and non-implanted stents of the same surface treatment group. This ratio aided in understanding whether explanted stents had altered elemental compositions compared to non-implanted stents. After the initial inspection, a

single explanted stent from each processing type was sonicated for 10 min in ultra pure DI water, allowed to dry, and re-evaluated using SEM and EDS.

2.5. Statistics

ASTM F2129 rest potentials were analyzed statistically using one way Analysis of Variance (ANOVA). Since some stents did not experience breakdown during ASTM F2129 testing, breakdown potentials and over potentials were analyzed using log-rank analysis specific for right censored data. Student's *t*-tests were used to compare the Ni/Ti ratios of non-implanted and explanted stents from the same processing group. P-values less than 0.05 were considered statistically significant.

3. Results

3.1. In-vitro oxide layer and pitting characterization

Surface processing resulted in visually different colors for each stent group indicating unique oxide layers (Table 1). SP stents were dark in appearance and possessed a thick oxide (420 nm) with a nickel-rich region below the titanium oxide layer (Fig. 1). In contrast, MP stents had a bright, shiny metallic appearance with a thin oxide (4 nm) and no nickel-rich layer present. AF stents were metallic blue in appearance and possessed an approximately 130 nm thick oxide, with the slight presence of a nickel-rich layer. OT stents were dull and dark in appearance and had a similar Auger profile to SP stents, with a nickel-rich region below the titanium oxide layer (399 nm).

Pitting corrosion testing per ASTM F2129 demonstrated the potentiodynamic behavior was distinctly different between SP, MP, AF, and OT stent processing groups (Fig. 2). MP and AF stents had similar rest potentials ($p = 0.747$), and were approximately 100 mV more anodic compared to SP and OT stents (Fig. 3). Rest potentials for MP stents were statistically greater compared to SP and OT stents ($p < 0.033$). SP stents exhibited the highest pitting corrosion resistance, where only 1/14 (7%) stents exhibited breakdown. MP stents had the second highest breakdown potentials with 10/14 (71%) stents exhibiting breakdown. All AF stents (14/14) experienced breakdown and had substantially lower breakdown potentials than SP and MP stents. Similarly all OT stents (8/8) experienced breakdown and had the lowest values compared to the other groups. The breakdown and overpotentials for each stent group were statistically different from each other ($p \leq 0.001$), except for AF and OT stents. While the breakdown potentials for OT stents were significantly lower than AF stents ($p = 0.026$), the overpotential values were similar to each other ($p = 0.309$).

3.2. In-vivo corrosion analysis

No visual or elemental evidence of pitting corrosion was observed in explanted SP and MP stents; both stents displayed a similar morphology to their respective non-implanted stents (Fig. 4). All non-implanted stents had inherent manufacturing features, such as voids. MP stents had smooth consistent surfaces throughout. SP stents were not as smooth and contained areas of fine surface cracks at the intrados, likely due to the crimping and deployment process (Fig. S2). While the cracks remained in explanted SP stents, corrosion was not evident in those cracked areas. Ni/Ti ratios of non-implanted SP stents (1.12 ± 0.06, $n = 13$) were not significantly different ($p = 0.470$) from explants (1.11 ± 0.03, $n = 47$). Similarly, Ni/Ti ratios for MP non-implanted stents (1.11 ± 0.01, $n = 14$) were not significantly different ($p = 0.878$) from explants (1.13 ± 0.04, $n = 36$) (Fig. 5).

In contrast to SP and MP stents, explanted AF stents displayed distinct areas of corrosion compared to their non-implanted controls (Fig. 6). Non-implanted AF stents had more apparent superficial inclusions (inherent to the material) and fine cracks at the

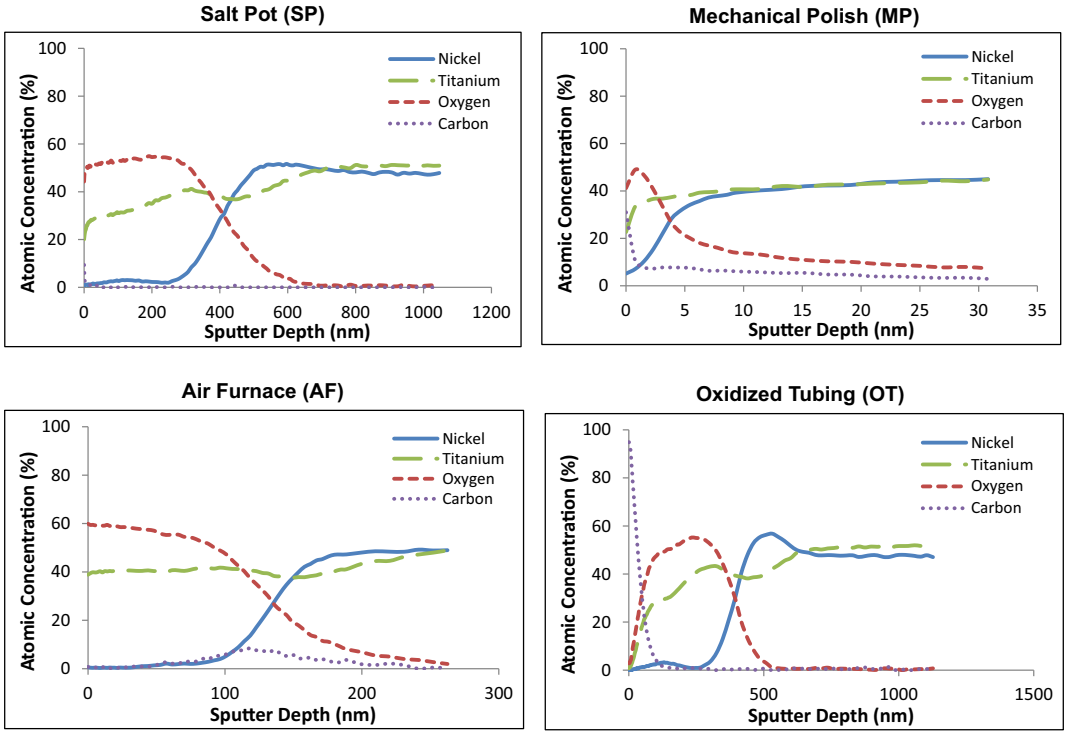

Fig. 1. Auger depth plots of different stent surfaces displaying oxide layer chemistry and composition. Oxide layer thickness was determined using full width at half maximum method: SP 420 nm; MP 4 nm; AF 130 nm; OT 399 nm (n = 1 per stent type).

Please cite this article in press as: S.J.L. Sullivan et al., The effects of surface processing on *in-vivo* corrosion of Nitinol stents in a porcine model, Acta Biomater. (2017), http://dx.doi.org/10.1016/j.actbio.2017.08.029

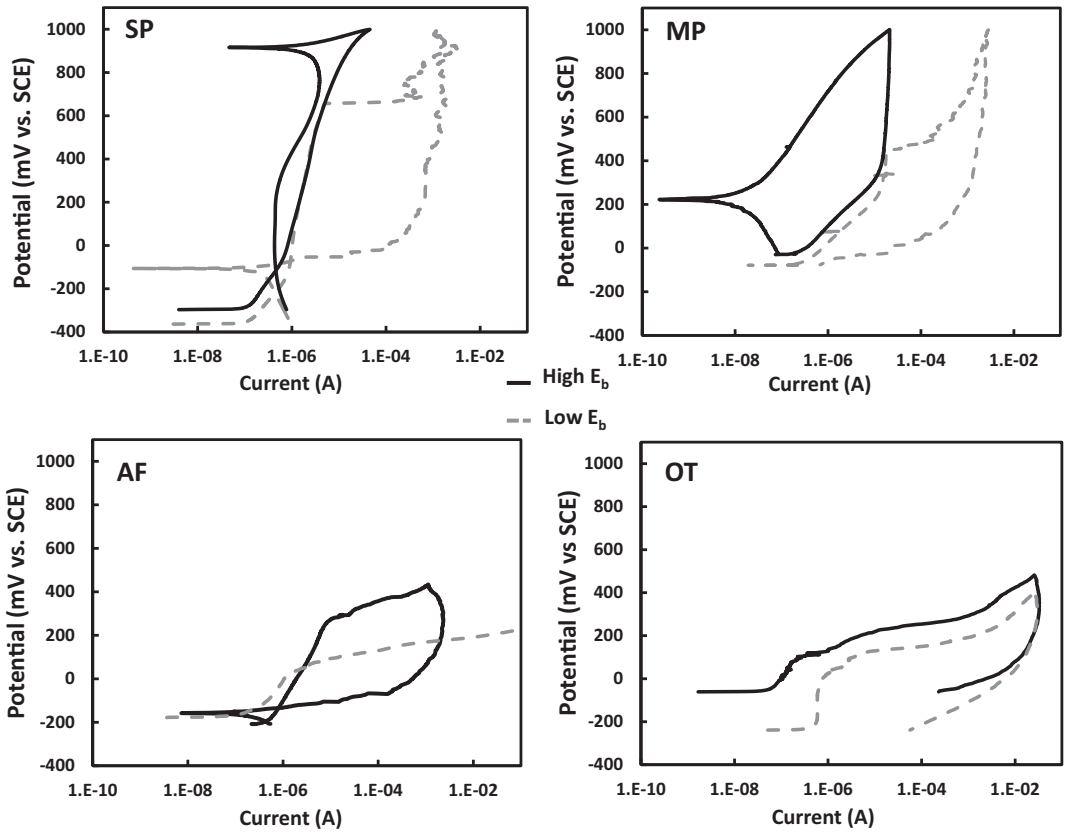

Fig. 2. Potentiodynamic polarization curves for SP, MP, AF, and OT stents displaying the minimum breakdown (dotted gray line) and maximum breakdown (black line).

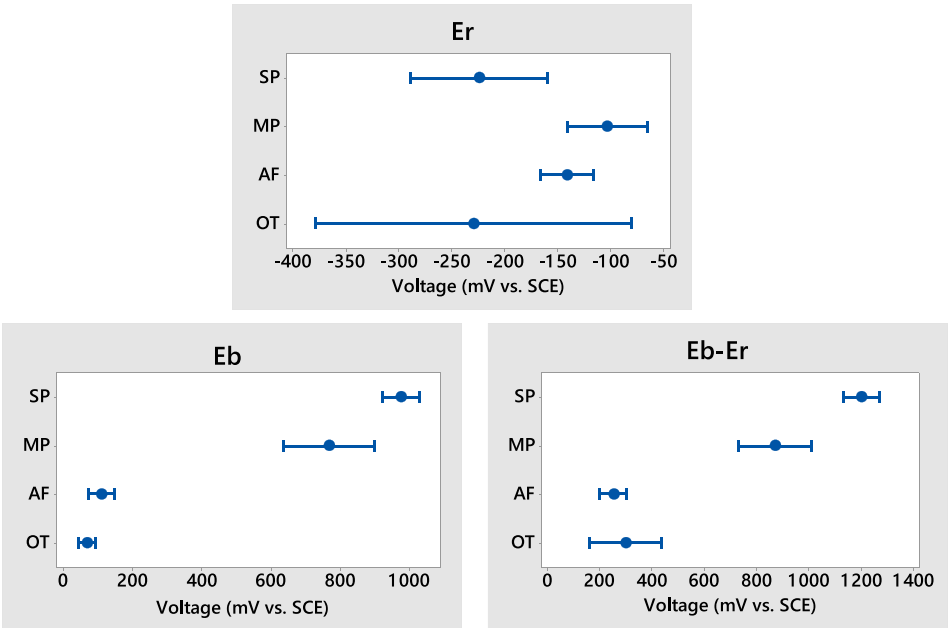

Fig. 3. 95% confidence interval plots for rest potential (Er), breakdown potential (Eb), and overpotential (Eb-Er) obtained from ASTM F2129 testing.

intrados compared to SP stents. Corrosion was observed predominately on the abluminal surface with variable morphology. Although more infrequent, corrosion without microcracks was detected in areas of expected low mechanical strain (Fig. 7a). Corrosion in retrieved AF stents was predominantly associated with extensive microcracks at the intrados of these stents and along connecting struts. Some microcracks were seen with "bubbling" of the oxide indicating potential subsurface corrosion (Fig. 7b). In severe cases, localized corrosion resulted in oxide delamination in areas with microcracks (Figs. 6 and 7c). In these regions, the exposed bulk metal was readily detected using backscattered mode during SEM imaging (Fig. 8). Average Ni/Ti ratio in regions

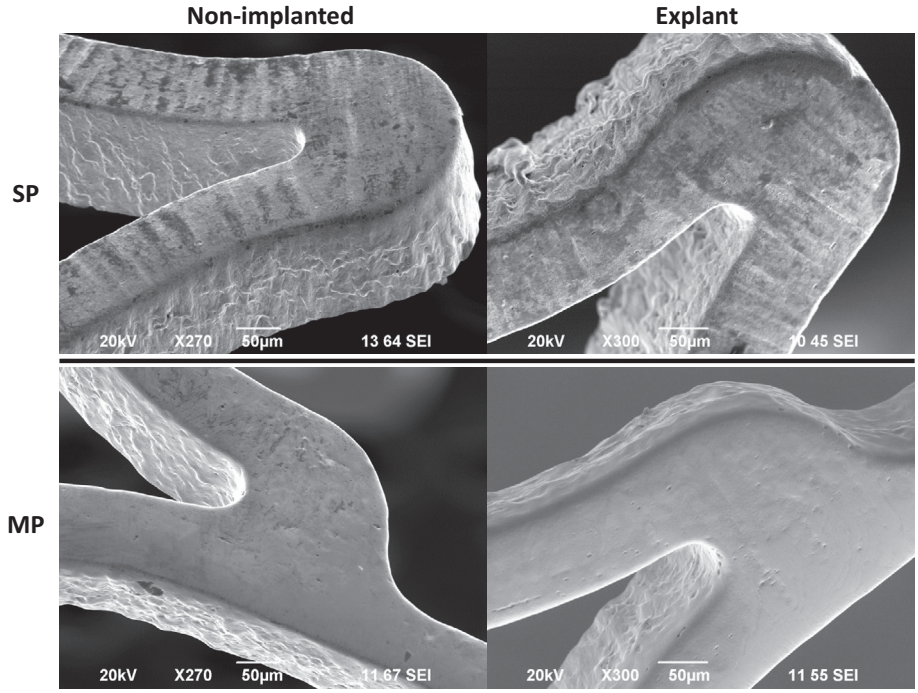

Fig. 4. Representative SEM images of (left) non-implanted control and (right) explanted salt pot (SP) and mechanically polished (MP) stents. Explanted stent surfaces appeared similar to non-implanted stents and free from detectable corrosion.

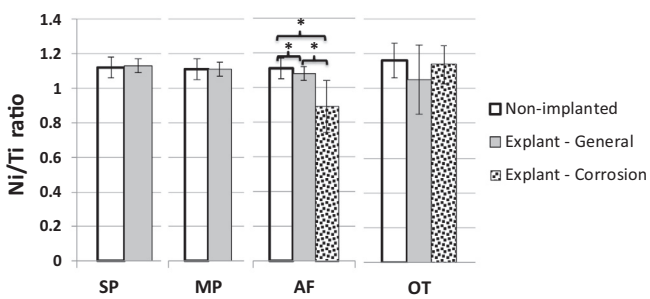

Fig. 5. Ni/Ti ratios of SP, MP, AF, and OT stents. Areas of analysis were visually free from detectable corrosion (non-implanted and explant-general) or within corroded areas (explant-corrosion). *Denotes significance difference between groups ($p \leq 0.05$) Baseline samples: minimum n = 12; Explant samples: minimum n = 22.

that appeared non-corroded (1.08 ± 0.06, n = 22) was approximately 3% lower ($p = 0.018$) compared to non-implanted AF stents (1.12 ± 0.02, n = 12). Ni/Ti ratios in visually corroded areas of AF explants (0.89 ± 0.15, n = 24) was 17–20% lower than non-implanted stents and in areas of explants that did not appear corroded ($p \leq 0.001$, Fig. 5).

The surface appearance of OT non-implanted stents was substantially rougher than other stent groups with noticeable drawing lines and scratches likely due to limited surface processing (Fig. 9). Sonication of the explanted OT stents exposed large pits on the abluminal surface that penetrated into the bulk Nitinol material and were accompanied by micro-pits in the surrounding oxide layer (Fig. 10). However, there were no significant visual or EDS changes due to sonication for OT non-implanted stents. On some areas of OT explants, pits had coalesced to corrode nearly the entire width of the stent strut (Fig. 11). Ni/Ti ratios in areas without visible corrosion (1.05 ± 0.31, n = 32) were lower than corresponding areas in non-implanted stents (1.16 ± 0.10, n = 20), but were not significantly different ($p = 0.095$). Ni/Ti ratios for pitted areas (1.14 ± 0.11, n = 59) were not significantly different than non-corroded surfaces on explanted and non-implanted stents ($p \geq 0.162$, Fig. 5).

4. Discussion

Cardiovascular device manufacturers commonly assess corrosion resistance of their metallic implants prior to clinical use. However, a major limitation during this evaluation is the lack of data to correlate *in-vitro* with *in-vivo* corrosion performance. In particular, it is unclear how corrosion resistance measured by breakdown potentials in ASTM F2129 testing relates to actual corrosion resistance of a device under clinical use. Our study addressed this knowledge gap by correlating bench testing with *in-vivo* observations of corrosion in stents processed to have unique surface properties. The results indicate that stents manufactured to have breakdown potentials less than approximately 200 mV (based on 95% confidence intervals) displayed evidence of localized corrosion *in-vivo*. Furthermore, we found that stents with breakdown potentials above approximately 600 mV (based on 95% confidence intervals) were free from detectable corrosion after 6 months *in-vivo*. Although these results are in good agreement with previously published acceptance criteria [49], a clinically relevant assessment of an implant's corrosion resistance should include results from corrosion bench testing and a thorough understanding of a device's surface chemistry, composition. For example, OT stents were intentionally fabricated with minimal processing (e.g. no grinding/honing of raw tubing or final polishing or passivation) as a worst case scenario to determine if corrosion would be observed *in-vivo*. These stent surfaces were very rough and had a dark appearance similar to Nitinol wires with a black oxide. In addition, metallographic cross sections of OT stent struts revealed substantial variability of the oxide thickness (approximately 200 to 1000 nm, Fig. S3). As a result, OT stents possessed the lowest breakdown potentials *in-vitro* and the oxide layer was unable to protect the implant from the *in-vivo* electrochemical environment as evidenced by extensive pitting observed on the explanted stent's

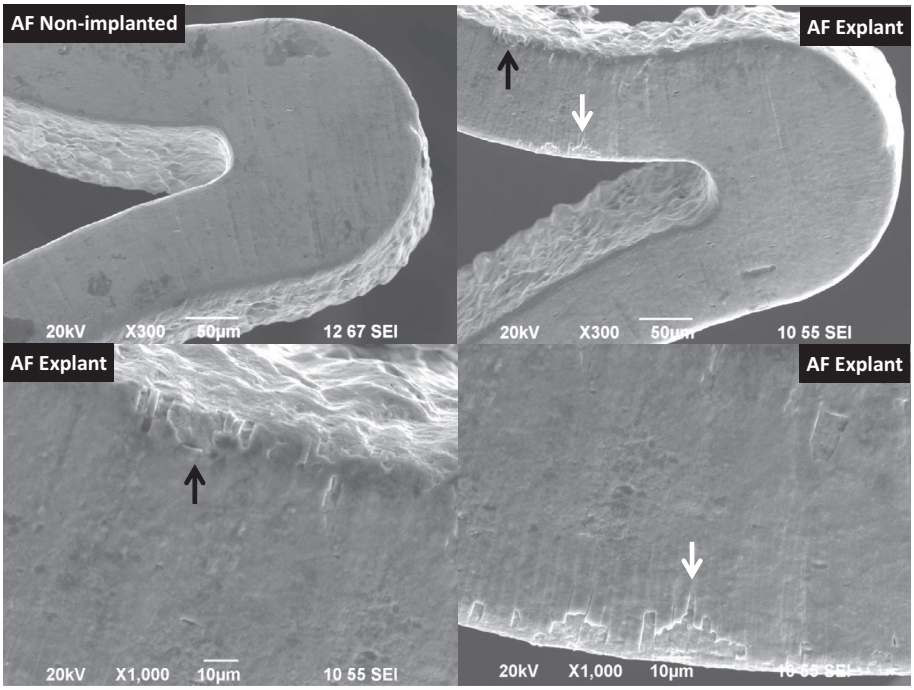

Fig. 6. Representative SEM images of (top left) non-implanted control and (top right) explant of air furnace (AF) stent. Magnification revealed cracking and corrosion exposing the substrate (bottom right) along the stent edge and (bottom left) at the intrados.

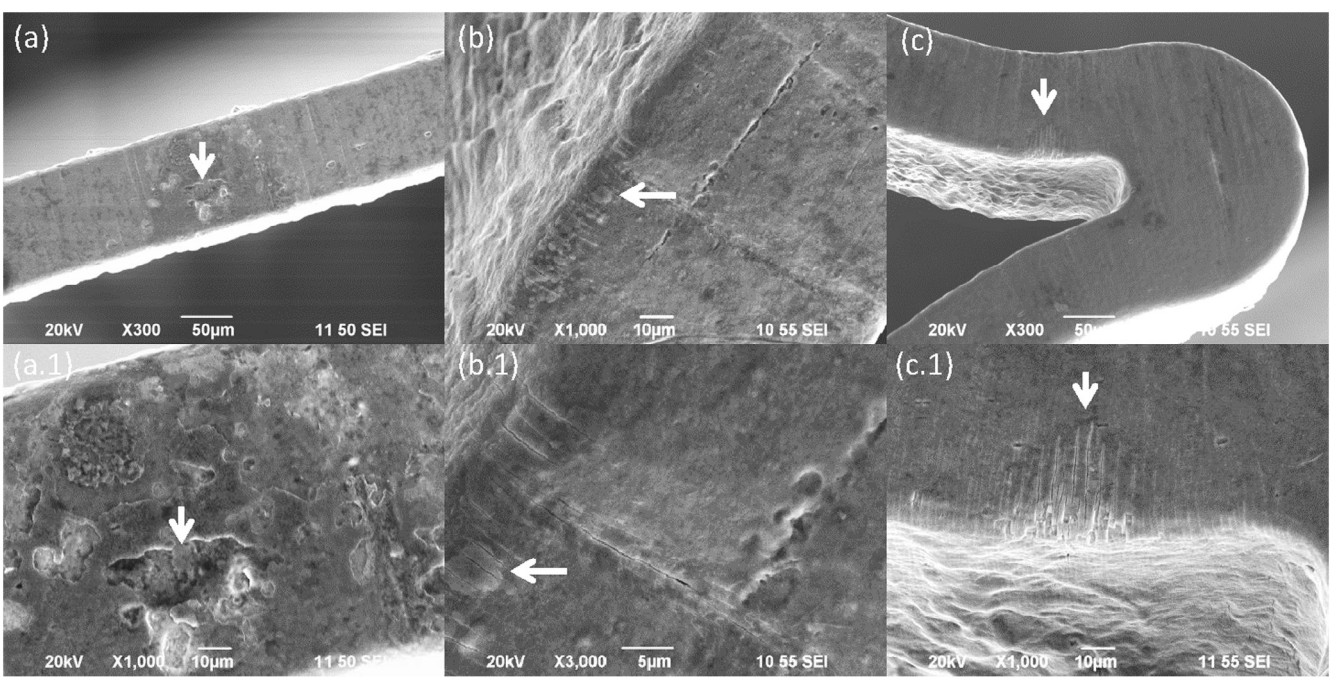

Fig. 7. Examples of different corrosion morphologies observed in explanted air furnace (AF) stents. (a) corrosion without surrounding cracks (b) delamination initiation where cracks allowed "bubbling" of the oxide (potential subsurface corrosion) (c) "halo" of corrosion with cracking and oxide delamination at intradose. Magnified images of each location shown below (a.1–c.1).

struts. In fact, focused ion beam milling on one of these areas found pits to be up to 9 µm deep. Although pitting was visually evident, Ni/Ti ratios in these areas were similar to non-implanted and visually non-corroded regions of explants suggesting deep pitting into the bulk metal.

In contrast to OT stents, AF stents incorporated common processing methods to remove the original oxide from the raw tubing as well as remove the heat affected zone post laser cutting. However, stents were heat treated in a box furnace in air without final polishing and/or passivation. The resulting moderately thick thermal oxide was blue in appearance, similar to a first generation laser-cut Nitinol stent (Fig. S4). AF stents also possessed the next lowest breakdown potentials and displayed localized corrosion *in-vivo*. Corroded areas in AF explants did not have classic pitting morphology as observed in the OT stents, rather regions of the oxide had delaminated from the surface indicating subsurface cor-

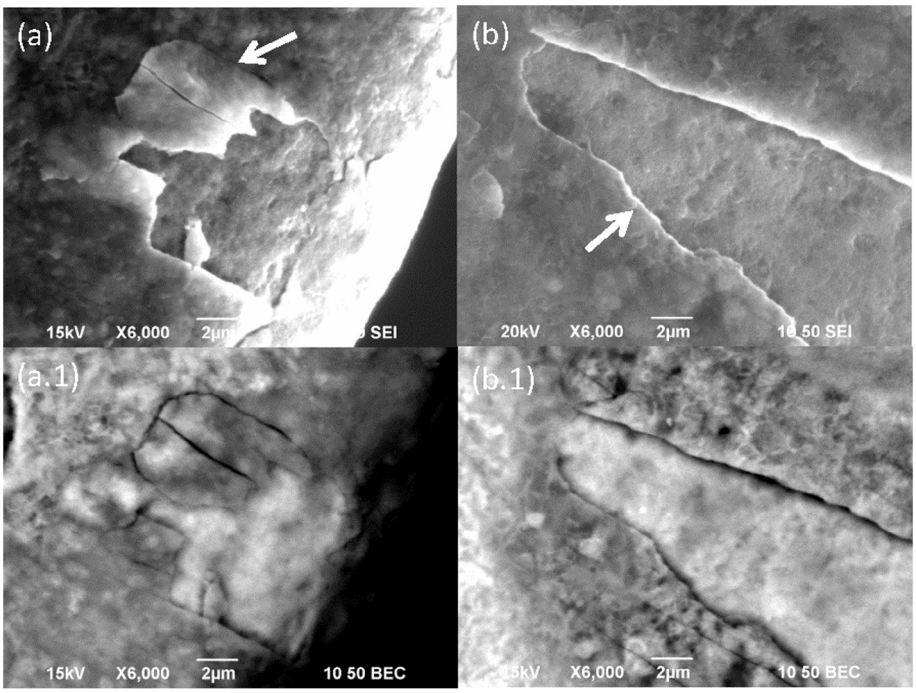

Fig. 8. High magnification examples of corrosion in air furnace (AF) stents with (a) oxide layer partially intact where crack sites have allowed subsurface corrosion and (b) full delamination of the oxide from the surface. Respective backscatter electron composite images (a.1 and b.1) show dark gray regions as oxide and brighter areas as exposed base metal.

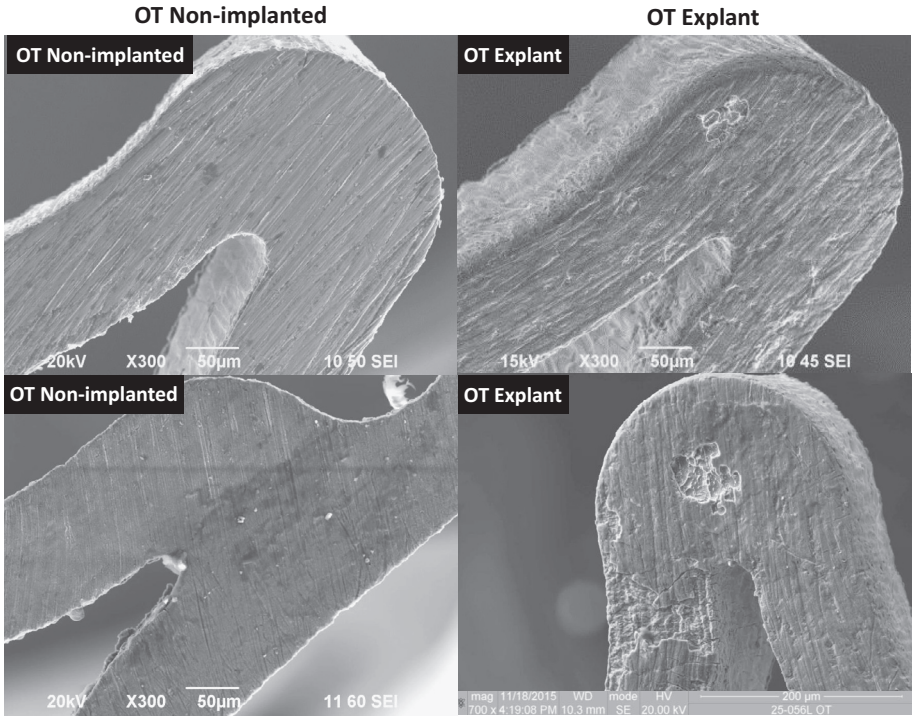

Fig. 9. Representative SEM images of oxidized tubing (OT) stents (left) non-implanted control and (right) sonnicated explant.

rosion. Although we found corrosion in areas without microcracks (expected low strain), the majority of corrosion occurred in areas of microcracking (high expected strain), which may be a result of combined mechanical and chemical mechanisms. We hypothesize that the mechanical damage (i.e. microcracking) may have provided a conduit for fluid to penetrate into nickel-rich regions or the bulk metal. Here, electrochemical interactions resulted in subsurface corrosion and in many instances delaminated localized areas of the oxide layer. These fully delaminated areas appeared to have selective dissolution of nickel, indicated by significantly lower Ni/Ti ratios compared to visually non-corroded regions on explants. However, Ni/Ti ratios in explanted areas where cracking was present without delamination had considerable variability (1.11–0.65), suggesting different stages of surface degradation

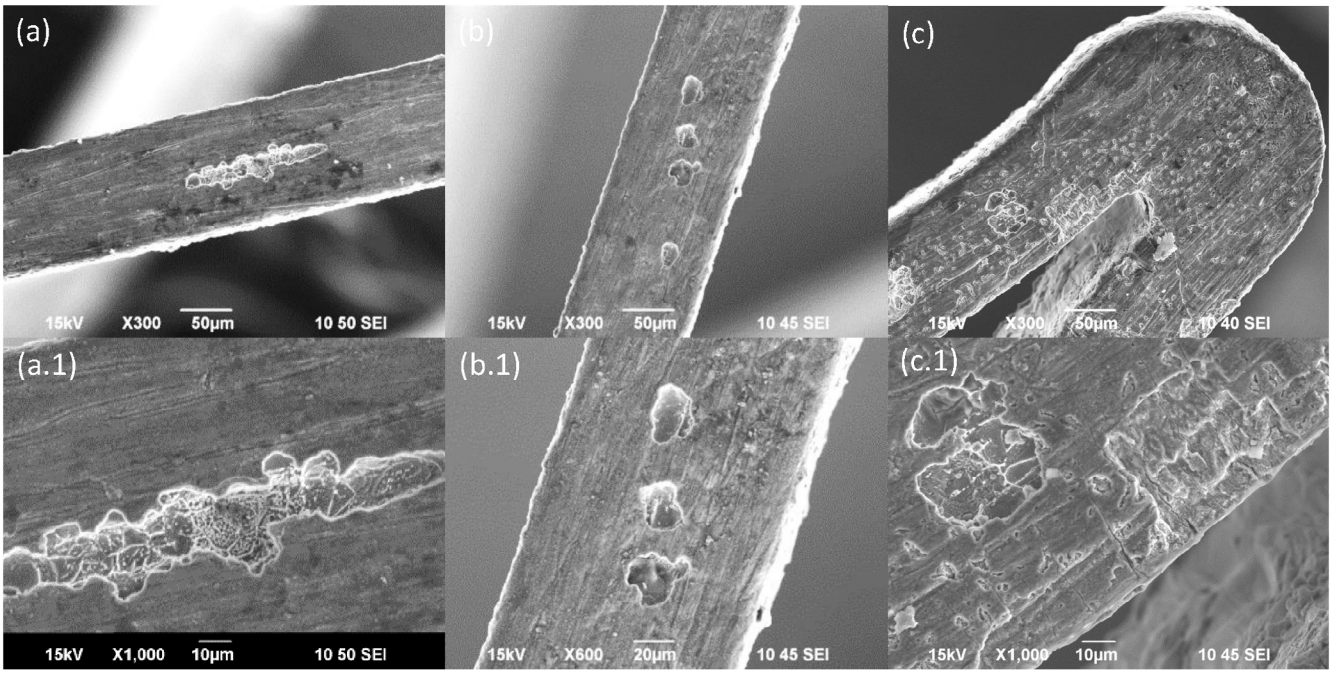

Fig. 10. Representative images of deep pitting observed in oxidized tubing (OT) stents (a–c). Magnified images of each location shown below (a.1–c.1).

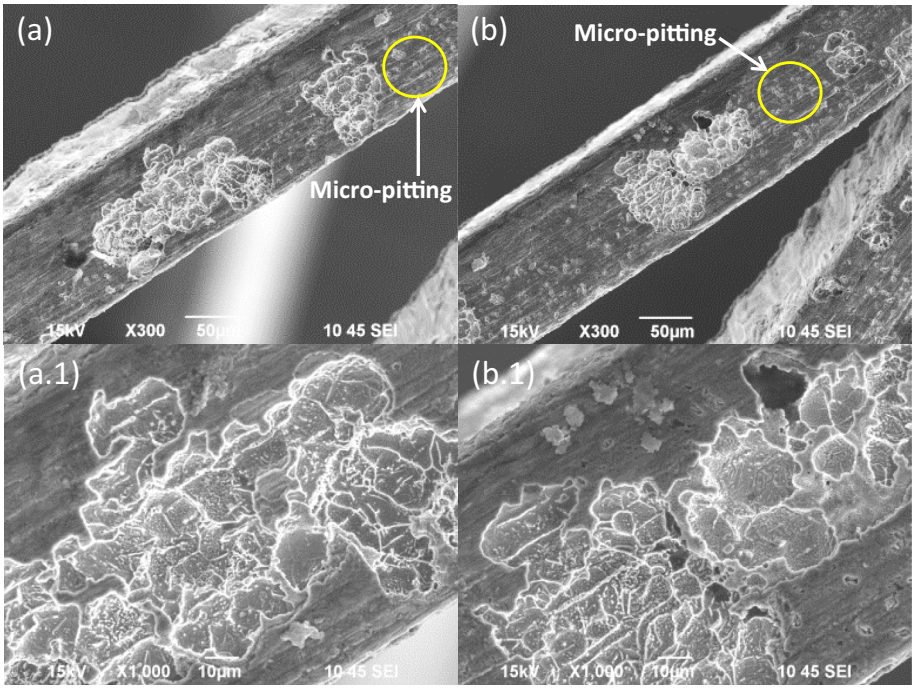

Fig. 11. Examples of micro-pitting (yellow circles) adjacent to areas of extensive corrosion in oxidized tubing (OT) stents (a–b). Magnified images of each location shown below (a.1–b.1). (For interpretation of the references to colour in this figure legend, the reader is referred to the web version of this article.)

were present in this group. This supports a previous finding that mechanical damage from strains exerted on the thermal oxide layer during loading and delivery of implants may reduce corrosion resistance [50]. If implantation duration was extended beyond 6 months, these degraded areas on the AF stent may have progressed to full delamination. In addition, definitively identifying corrosion, particularly features that do not appear as classical rounded pits, may require comparisons to non-implanted controls and/or chemical assessments within and outside of corroded areas.

MP stents were the only group in this study to use polishing as final processing steps to remove thermal oxides from previous heat treatments. Polishing is a commonly used final surface processing method for laser-cut stents as previous literature has shown that proper polishing of Nitinol preferentially removes surface nickel and produces a thin pure titanium oxide layer resulting in higher *in-vitro* corrosion resistance compared to thermal oxides with nickel-rich phases [46,51,52]. MP stents in this study had a shiny silver metallic appearance, indicative of a thin oxide, with no

nickel-rich regions detected from Auger depth profiles. Although MP stents displayed a wide range of breakdown potentials (approximately 500 mV to no breakdown), explanted devices demonstrated good corrosion resistance for 6 months *in-vivo*. Electropolished stents originally considered for this study possessed similar appearance, oxide layer depth and Auger profile as the MP stents, and were therefore not included in this study as we expected these stents would have similar or better corrosion resistance compared to MP stents.

SP stents were also free from detectable corrosion after 6 months of implantation. This is particularly noteworthy since the SP stent had a complex thermal oxide that was approximately 100 times thicker than MP stents. The thick oxide layer in SP stents was effective at deterring pitting as demonstrated by the lack of breakdown in 93% of SP stents tested per ASTM F2129. Interestingly, *in-vivo* corrosion was not observed in SP stents even with microcracks present. This result may be because the cracks remained in the oxide layer due to the substantially thicker oxide. However, these cracks can expose nickel-rich regions and lead to greater release of nickel into the bloodstream and surrounding vasculature due to its thick complex oxide. In fact, our previous *in-vitro* immersion study found SP stent had a significantly higher nickel release than AF and MP stents [41]. The SP's thick oxide was beneficial in resisting pitting corrosion, but not thin enough to withstand crimping strains resulting in cracking and leaching of nickel from the stent. Taken together, these results highlight the importance of oxide layer chemistry and composition on localized and general corrosion. Interestingly, OT stents had similarly thick thermal oxides to SP stents; however, the *in-vitro* breakdown potentials and *in-vivo* corrosion resistance were drastically different. We suspect that processes to remove of the original tubing oxide and heat affected zones in SP stents greatly improved bench and *in-vivo* corrosion resistance.

There are limitations that must be considered when interpreting results from this study. Processing was not inclusive of all steps (e.g. passivation) typical for finished Nitinol stents. This was necessary to intentionally manufacture stents with targeted pitting corrosion resistance. Our study provided insight into the short term (6 months) corrosion resistance of uniquely processed Nitinol stents. However, cardiovascular stents are intended to be implanted for a minimum of 10 years. Therefore, the longer term corrosion susceptibility of these stent groups remains unclear, particularly for SP stents that had a thick thermal oxide. Longer exposure of SP stents to the dynamic electrochemical environment may degrade the passive layer over time. Another limitation is that we were not able to correlate *in-vivo* corrosion to the full spectrum of breakdown potentials in ASTM F2129 testing. Our attempts to produce a stent group with *in-vitro* breakdown potentials between approximately 300 and 500 mV were unsuccessful due to high variability. Nevertheless, understanding the *in-vivo* corrosion performance for this range (300–500 mV) is important to fully establish an *in-vitro* to *in-vivo* corrosion relationship. In order to verify corroded areas, we complemented our visual analysis with EDS to understand whether chemical changes occurred. However, we acknowledge EDS incorporates both surface oxide and substrate material (approximately 1 μm depth into surface for the parameters used). In order to minimize this limitation, precautions were taken to maintain consistent sample angle and parameter settings to create more clear comparisons between explants and non-implanted controls. Finally, this study did not address the biological consequences of localized corrosion observed in explants. Future work is focused on understanding the clinical sequelae from corrosion byproducts released into surrounding arterial tissue and whether there is an inflammatory response around stent struts.

Table 2
Stent performance summary.

	SP	MP	AF	OT
Visual Appearance				
E_b (mV)	974.8 ± 94.3	767.1 ± 225.5	110.6 ± 63.2	67.5 ± 29.3
E_r (mV)	−224.3 ± 112.4	−103.1 ± 65.1	−141.3 ± 43.7	−229.5 ± 178.1
E_b–E_r (mV)	1199.1 ± 118.3	870.2 ± 240.3	252.0 ± 89.5	296.9 ± 164.5
Non-implanted Ni/Ti (%wt/wt)	1.12 ± 0.06	1.11 ± 0.01	1.12 ± 0.02	1.16 ± 0.01
Oxide Layer Thickness (nm)	420	4	130	399
Explant Corrosion?	No	No	Yes	Yes

Please cite this article in press as: S.J.L. Sullivan et al., The effects of surface processing on *in-vivo* corrosion of Nitinol stents in a porcine model, Acta Biomater. (2017), http://dx.doi.org/10.1016/j.actbio.2017.08.029

5. Conclusions

This was the first controlled study to correlate *in-vitro* corrosion testing with *in-vivo* corrosion performance of cardiovascular stents. We found that Nitinol stent groups with breakdown potentials lower than 200 mV displayed *in-vivo* corrosion after 6 months of implantation. Conversely, Nitinol stents with pits initiating at potentials higher than approximately 600 mV showed no signs of *in-vivo* corrosion after 6 months of implantation. Table 2 provides a summary of each stent group with bench characterization and *in-vivo* corrosion performance. These findings demonstrate that accurately predicting corrosion resistance *in-vivo* involves incorporating functional testing results (e.g. ASTM F2129) with a detailed understanding of the relationship between surface processing and the resulting oxide layer composition and chemistry.

Acknowledgements

This study was made possible by funding from FDA's Critical Path Initiative (2012–2015) and a research collaborative agreement established between FDA and Nitinol Devices and Components (now Confluent Medical Technologies). This project was also supported in part by an appointment to the Oak Ridge Institute for Science and Education (ORISE) Research Participation Program at FDA/CDRH, administered by ORISE through an interagency agreement between the U.S. Department of Energy and FDA/CDRH. The authors also acknowledge FDA's Advanced Characterization Facility, particularly John Bouck, Jiwen Zheng and Yong Wu for aid in electron microscopy.

Disclaimer.

The mention of commercial products, their sources, or their use in connection with materials reported herein is not to be construed as either an actual or implied endorsement of such products by the Department of Health and Human Services.

Disclosure

The authors have no known conflicts of interest associated with this publication.

Appendix A. Supplementary data

Supplementary data associated with this article can be found, in the online version, at http://dx.doi.org/10.1016/j.actbio.2017.08.029.

References

[1] B. Bolland, D. Culliford, D. Langton, J. Millington, N. Arden, J. Latham, High failure rates with a large-diameter hybrid metal-on-metal total hip replacement clinical, radiological and retrieval analysis, J. Bone Joint Surg. Br. 93 (2011) 608–615.
[2] K.B. Fricka, H. Ho, W.J. Peace, C.A. Engh, Metal-on-metal local tissue reaction is associated with corrosion of the head taper junction, J. Arthroplasty 27 (2012) 26–31.
[3] J.R. Goldberg, J.L. Gilbert, J.J. Jacobs, T.W. Bauer, W. Paprosky, S. Leurgans, A multicenter retrieval study of the taper interfaces of modular hip prostheses, Clin. Orthop. Relat. Res. 401 (2002) 149–161.
[4] J.L. Gilbert, C.A. Buckley, J.J. Jacobs, In vivo corrosion of modular hip prosthesis components in mixed and similar metal combinations. The effect of crevice, stress, motion, and alloy coupling, J. Biomed. Mater. Res. 27 (1993) 1533–1544.
[5] S.M. Kurtz, S.B. Kocagöz, J.A. Hanzlik, R.J. Underwood, J.L. Gilbert, D.W. MacDonald, G.-C. Lee, M.A. Mont, M.J. Kraay, G.R. Klein, Do ceramic femoral heads reduce taper fretting corrosion in hip arthroplasty? A retrieval study, Clin. Orthop. Relat. Res. 471 (2013) 3270–3282.
[6] Y. Tomizawa, T. Hanawa, D. Kuroda, H. Nishida, M. Endo, Corrosion of stainless steel sternal wire after long-term implantation, J. Artif. Org. 9 (2006) 61–66.
[7] Y. Tomizawa, T. Hanawa, Corrosion of pure titanium sternal wire, Ann. Thorac. Surg. 84 (2007) 1012–1014.
[8] R. Gray, Metallographic examinations of retrieved intramedullary bone pins and bone screws from the human body, J. Biomed. Mater. Res. 8 (1974) 27–38.
[9] C. Heintz, G. Riepe, L. Birken, E. Kaiser, N. Chakfe, M. Morlock, G. Delling, H. Imig, Corroded nitinol wires in explanted aortic endografts: An important mechanism of failure?, J Endovasc. Ther. 8 (2001) 248–253.
[10] G. Riepe, C. Heintz, E. Kaiser, N. Chakfe, M. Morlock, M. Delling, H. Imig, What can we learn from explanted endovascular devices?, Eur J. Vasc. Endovasc. Surg. 24 (2002) 117–122.
[11] B.C. Brott, D. Halwani, P.G. Anderson, A.S. Anayiotos, J.E. Lemons, Scanning electron microscopy analysis of corrosion of stainless steel and nitinol Stents from autopsy retrievals, J. Am. Coll. Cardiol. 51 (2008). B92-B.
[12] D.O. Halwani, P.G. Anderson, J.E. Lemons, W.D. Jordan, A.S. Anayiotos, B.C. Brott, In-vivo corrosion and local release of metallic ions from vascular stents into surrounding tissue, J. Invasive Cardiol. 22 (2010) 528–535.
[13] D.O. Halwani, P.G. Anderson, B.C. Brott, A.S. Anayiotos, J.E. Lemons, Surface characterization of explanted endovascular stents: evidence of in vivo corrosion, J. Biomed. Mater. Res. Part B: Appl. Biomater. 95B (2010) 225–238.
[14] Y.-M. Kwon, S.J. Ostlere, P. McLardy-Smith, N.A. Athanasou, H.S. Gill, D.W. Murray, "Asymptomatic" pseudotumors after metal-on-metal hip resurfacing arthroplasty: prevalence and metal ion study, J. Arthroplasty 26 (2011) 511–518.
[15] P. Campbell, E. Ebramzadeh, S. Nelson, K. Takamura, K. De Smet, H.C. Amstutz, Histological features of pseudotumor-like tissues from metal-on-metal hips, Clin. Orthop. Rel. Res. 468 (2010) 2321–2327.
[16] H.J. Cooper, C.J. Della Valle, R.A. Berger, M. Tetreault, W.G. Paprosky, S.M. Sporer, J.J. Jacobs, Corrosion at the head-neck taper as a cause for adverse local tissue reactions after total hip arthroplasty, J. Bone Joint Surg. 94 (2012) 1655–1661.
[17] H.J. Cooper, R.M. Urban, R.L. Wixson, R.M. Meneghini, J.J. Jacobs, Adverse local tissue reaction arising from corrosion at the femoral neck-body junction in a dual-taper stem with a cobalt-chromium modular neck, J. Bone Joint Surg. Am. 95 (2013) 865–872.
[18] D. Langton, T. Joyce, S. Jameson, J. Lord, M. Van Orsouw, J. Holland, A. Nargol, K. De Smet, Adverse reaction to metal debris following hip resurfacing the influence of component type, orientation and volumetric wear, J. Bone Joint Surg. Br. 93 (2011) 164–171.
[19] M. Santin, L. Mikhalovska, A.W. Lloyd, S. Mikhalovsky, L. Sigfrid, S.P. Denyer, S. N. Field, D. Teer, In vitro host response assessment of biomaterials for cardiovascular stent manufacture, J. Mater. Sci. Mater. Med. 15 (2004) 473–477.
[20] J.C. Wataha, N.L. O'Dell, B.B. Singh, M. Ghazi, G.M. Whitford, P.E. Lockwood, Relating nickel-induced tissue inflammation to nickel release in vivo, J. Biomed. Mater. Res. 58 (2001) 537–544.
[21] J.P. Thyssen, A. Linneberg, T. Menne, J.D. Johansen, The epidemiology of contact allergy in the general population - prevalence and main findings, Contact Dermatitis 57 (2007) 287–299.
[22] WHO, Arsenic, metals, fibres, and dusts: a review of human carcinogens, IARC Monographs 100C (2012) 169–218.
[23] P.H. Gitlitz, F.W. Sunderman Jr., P.J. Goldblatt, Aminoaciduria and proteinuria in rats after a single intraperitoneal injection of Ni(II), Toxicol. Appl. Pharmacol. 34 (1975) 430–440.
[24] M.C. Pereira, M.L. Pereira, J.P. Sousa, Evaluation of nickel toxicity on liver, spleen, and kidney of mice after administration of high-dose metal ion, J. Biomed. Mater. Res. 40 (1998) 40–47.
[25] A. Lyell, W.H. Bain, R.M. Thomson, Repeated failure of nickel-containing prosthetic heart-valves in a patient allergic to nickel, Lancet 2 (1978) 657–659.
[26] A. Gimenez-Arnau, V. Riambau, E. Serra-Baldrich, J.G. Camarasa, Metal-induced generalized pruriginous dermatitis and endovascular surgery, Contact Dermatitis 43 (2000) 35–40.
[27] L. Slavin, J.M. Tobis, K. Rangarajan, C. Dao, J. Krivokapich, D.S. Liebeskind, Five-year experience with percutaneous closure of patent foramen ovale, Am. J. Cardiol. 99 (2007) 1316–1320.
[28] G. Honari, S.G. Ellis, B.L. Wilkoff, M.A. Aronica, L.G. Svensson, J.S. Taylor, Hypersensitivity reactions associated with endovascular devices, Contact Dermatitis 59 (2008) 7–22.
[29] K.H. Kim, J.C. Park, N.S. Yoon, J.Y. Moon, Y.J. Hong, H.W. Park, J.H. Kim, Y. Ahn, M.H. Jeong, J.G. Cho, J.C. Kang, A case of allergic contact dermatitis following transcatheter closure of patent ductus arteriosus using Amplatzer ductal occluder, Int. J. Cardiol. 127 (2008) E98–E99.
[30] N.G. Kounis, G. Hahalis, S.A. Kounis, G.N. Kounis, Kounis syndrome and hypersensitivity reactions associated with endovascular devices, Contact Dermatitis 60 (2009) 121–122.
[31] P. Jetty, S. Jayaram, J. Veinot, M. Pratt, Superficial femoral artery nitinol stent in a patient with nickel allergy, J. Vasc. Surg. (2013).
[32] R. Köster, D. Vieluf, M. Kiehn, M. Sommerauer, J. Kähler, S. Baldus, T. Meinertz, C.W. Hamm, Nickel and molybdenum contact allergies in patients with coronary in-stent restenosis, Lancet 356 (2000) 1895–1897.
[33] S.N. Rosenbloom, R. Corbett, An assessment of ASTM F2129 electrochemical testing of small medical implants-lessons learned, in: Proceedings of the NACE Corrosion Conference & Exposition, Nashville, TN, USA, 2007, pp. 11–15.
[34] T.P. Hoar, D.C. Mears, Corrosion-resistant alloys in chloride solutions – materials for surgical implants, Proc. R. Soc. Lond. Ser. A: Math. Phys. Sci. 294 (1966) 486–1000.

[35] C.C. Shih, S.J. Lin, K.H. Chung, Y.L. Chen, Y.Y. Su, Increased corrosion resistance of stent materials by converting current surface film of polycrystalline oxide into amorphous oxide, J. Biomed. Mater. Res. 52 (2000) 323–332.
[36] L.B. Pertile, P.M.S. Silva, V.B. Peccin, R. Peres, P.G. Silveira, C. Giacomelli, F.C. Giacomelli, M.C. Fredel, A. Spinelli, In vivo human electrochemical properties of a NiTi-based alloy (Nitinol) used for minimally invasive implants, J. Biomed. Mater. Res., Part A 89A (2009) 1072–1078.
[37] A.I. Munoz, J. Schwiesau, B. Jolles, S. Mischler, In vivo electrochemical corrosion study of a CoCrMo biomedical alloy in human synovial fluids, Acta Biomater. 21 (2015) 228–236.
[38] L.E. Eiselstein, D. Steffey, A. Nissan, N. Corlett, R. Dugnani, E. Kus, S.G. Stewart, Acceptance criteria for corrosion resistance of medical devices: statistical analysis of nitinol pitting in in vivo environments, J. Mater. Eng. Perform. 18 (2009) 768–780.
[39] B.G. Pound, Susceptibility of nitinol to localized corrosion, J. Biomed. Mater. Res., Part A 77 (2006) 185–191.
[40] S. Nagaraja, M. Di Prima, D. Saylor, E. Takai, Current practices in corrosion, surface characterization, and nickel leach testing of cardiovascular metallic implants, J. Biomed. Mater. Res., Part B: Appl. Biomater. (2016).
[41] S.J. Sullivan, M.L. Dreher, J. Zheng, L. Chen, D. Madamba, K. Miyashiro, C. Trépanier, S. Nagaraja, Effects of oxide layer composition and radial compression on nickel release in nitinol stents, Shape Mem. Superelast. 1 (2015) 319–327.
[42] B. Bhargava, N.K. Reddy, G. Karthikeyan, R. Raju, S. Mishra, S. Singh, R. Waksman, R. Virmani, B. Somaraju, A novel paclitaxel-eluting porous carbon–carbon nanoparticle coated, nonpolymeric cobalt–chromium stent: evaluation in a porcine model, Catheter. Cardiovasc. Interv. 67 (2006) 698–702.
[43] T.L.P. Slottow, R. Pakala, T. Okabe, D. Hellinga, R.J. Lovec, F.O. Tio, A.B. Bui, R. Waksman, Optical coherence tomography and intravascular ultrasound imaging of bioabsorbable magnesium stent degradation in porcine coronary arteries, Cardiovasc. Revasc. Med. 9 (2008) 248–254.
[44] R. Waksman, R. Pakala, R. Baffour, D. Hellinga, R. Seabron, F.O. Tio, E. Wittchow, M. Tittelbach, T. Diener, C. Harder, Efficacy and safety of pimecrolimus-eluting stents in porcine coronary arteries, Cardiovasc. Revasc. Med. 8 (2007) 259–274.
[45] S. Duda, B. Pusich, G. Richter, P. Landwehr, V. Oliva, A. Tielbeek, B. Wiesinger, J. Hak, H. Tielemans, G. Ziemer, E. Cristea, A. Lansky, J. Bérégi, Sirolimus-eluting stents for the treatment of obstructive superficial femoral artery disease: six-month results, Circulation 106 (2002) 1505–1509.
[46] B. Thierry, M. Tabrizian, C. Trepanier, O. Savadogo, L.H. Yahia, Effect of surface treatment and sterilization processes on the corrosion behavior of NiTi shape memory alloy, J. Biomed. Mater. Res. 51 (2000) 685–693.
[47] H.Q. Zhao, A. Nikanorov, R. Virmani, R. Jones, E. Pacheco, L.B. Schwartz, Late stent expansion and neointimal proliferation of oversized Nitinol stents in peripheral arteries, Cardiovasc. Interv. Radiol. 32 (2009) 720–726.
[48] S.J. Sullivan, P. Stafford, E. Malkin, M.L. Dreher, S. Nagaraja, Effects of tissue digestion solutions on surface properties of nitinol stents, J. Biomed. Mater. Res., Part B: Appl. Biomater. (2017).
[49] R.A. Corbett, Laboratory corrosion testing of medical implants, in: Proceedings of Materials and Processes for Medical Devices Conference ASM International, Materials Park, OH, 2004, pp. 166–171.
[50] L. Zhu, C. Trepanier, A. Pelton, J.M. Fino, Oxidation of Nitinol and its Effect on Corrosion Resistance, ASM Materials and Processes for Medical Devices, 2003.
[51] C. Trepanier, M. Tabrizian, L.H. Yahia, L. Bilodeau, D.L. Piron, Effect of modification of oxide layer on NiTi stent corrosion resistance, J. Biomed. Mater. Res. 43 (1998) 433–440.
[52] B. Clarke, W. Carroll, Y. Rochev, M. Hynes, D. Bradley, D. Plumley, Influence of nitinol wire surface treatment on oxide thickness and composition and its subsequent effect on corrosion resistance and nickel ion release, J. Biomed. Mater. Res., Part A 79 (2006) 61–70.

Please cite this article in press as: S.J.L. Sullivan et al., The effects of surface processing on *in-vivo* corrosion of Nitinol stents in a porcine model, Acta Biomater. (2017), http://dx.doi.org/10.1016/j.actbio.2017.08.029